ADVANCED MATERIALS INTERFACES
Open Access
www.advmatinterfaces.de

Carbon Monoxide Reduction Reaction to Produce Multicarbon Products in Acidic Electrolytes Using Gas Diffusion Electrode Loaded with Copper Nanoparticles

Ryo Kurihara, Kaito Nagita, Keitaro Ohashi, Yoshiharu Mukouyama, Takashi Harada, Shuji Nakanishi, and Kazuhide Kamiya**

The synthesis of multi-carbon products (C_{2+}) by electrochemical CO_2 reduction reaction (CO_2RR) is a promising technology that will contribute to the realization of a carbon-neutral society. In particular, efficient CO_2RR to produce C_{2+} in acidic electrolytes is desirable because the conversion of CO_2 to inert (bi)carbonate can be suppressed under acidic conditions, thereby increasing the efficiency of substrate CO_2 utilization. Herein, since C_{2+} products are produced via the dimerization of carbon monoxide, an intermediate in CO_2RR, the focus is on the carbon monoxide reduction reaction (CORR). A gas diffusion electrode loaded with copper nanoparticles is used in acidic electrolytes to investigate the conditions necessary for efficient C_{2+} production. The faradaic efficiency and partial current density for C_{2+} production attained 75% and 280 mA cm^{-2} in a pH 2.0 solution, and they reached up to 66% and 260 mA cm^{-2} even in a pH 1.0 solution. Numerical simulations showed that increasing the alkalinity of the electrode surface to greater than pH 7 by consuming protons is necessary to facilitate the production of C_{2+} during the CORR. When the desired level of alkalinity is achieved, the concentration and type of alkali cations present at the electrode surface have an impact on the selectivity for C_{2+} production.

1. Introduction

The electrochemical carbon dioxide (CO_2) reduction reaction (CO_2RR) has attracted much attention as a strategy to valorize anthropogenic CO_2.[1–4] For practical implementation of the CO_2RR, it is necessary to improve energy efficiency, product selectivity, and production rate.[5–7] One essential criterion for the social implementation of this technology is the production of higher-value chemicals at a high reaction rate, including multi-carbon compounds (C_{2+}, (e.g., ethylene, ethanol, acetic acid, and *n*-propanol)). Although non-Cu electrocatalysts for generating C_{2+} compounds have recently begun to be successfully developed,[8,9] Cu-based electrocatalysts have been the most extensively studied to efficiently produce these multicarbon compounds.[3,10–14] CO_2RR studies using Cu-based catalysts have generally been performed in neutral or alkaline electrolytes[15,16] because the competing H_2 evolution reaction (HER) tends to become dominant in acidic solutions. However, CO_2 is easily converted to inert (bi)carbonate, which migrates to the anode compartment or is discharged at the outlet of the anode compartment; thus, neutral or alkaline electrolytes are disadvantageous from the viewpoint of substrate utilization efficiency.[17–19] Therefore, an efficient CO_2RR that proceeds under acidic conditions is required.

R. Kurihara, K. Nagita, K. Ohashi, Y. Mukouyama, T. Harada, S. Nakanishi, K. Kamiya
Research Center for Solar Energy Chemistry
Graduate School of Engineering Science
Osaka University
1–3 Machikaneyama, Toyonaka, Osaka 560-8531, Japan
E-mail: nakanishi.shuji.es@osaka-u.ac.jp; kamiya.kazuhide.es@osaka-u.ac.jp

The ORCID identification number(s) for the author(s) of this article can be found under https://doi.org/10.1002/admi.202300731

Y. Mukouyama
Division of Science
College of Science and Engineering
Tokyo Denki University
Hatoyama, Saitama 350–0394, Japan

T. Harada, S. Nakanishi, K. Kamiya
Innovative Catalysis Science Division
Institute for Open and Transdisciplinary Research Initiatives (ICS-OTRI)
Osaka University
Suita, Osaka 565-0871, Japan

DOI: 10.1002/admi.202300731

The use of a gas diffusion electrode (GDE), which can overcome the problem of limited mass transport due to the low solubility of CO_2, has recently been reported to be an effective method to accelerate the CO_2RR.[20–22] For high-rate CO_2RR with GDEs, the local pH at the electrode surface increases with increasing cathodic current density, as both CO_2RR and HER consume protons. Therefore, the use of a GDE is expected to enable the CO_2RR to be conducted in acidic electrolytes. In fact, Huang et al. deposited a cation augmentation layer composed of cationic perfluorosulfonic acid ionomer onto the cathode surface; as a result, the CO_2RR was successfully conducted on a Cu catalyst at pH < 1 with a faradaic efficiency (FE) of 48% for multicarbon products at 1200 mAcm^{-2}.[23] Ma et al. reported that a high-alkalinity microenvironment was created when porous Cu nanosheets were used, resulting in an FE of 83.7% and a partial current density of 560 mA cm^{-2} for C_{2+}.[24] Our group also reported that Ni-doped covalent triazine frameworks (Ni-CTFs) on a GDE showed an FE greater than 90% for CO production from CO_2 in a solution at pH 2.[25] By contrast, when a normal immersed electrode was used, the FE was only 1.2% in an electrolyte with the same pH.[25] Several other groups have reported efficient electrochemical CO_2 reduction using acidic electrolytes.[18,26–34]

Although several studies have been conducted on the production of C_{2+} via CO_2RR in acidic solutions as mentioned above, the necessary conditions to improve its efficiency have not been fully elucidated, especially from a quantitative perspective. To obtain guidelines for enhancing C_{2+} production efficiency, we have turned our attention to the fact that the formation of C_{2+} products in the CO_2RR proceeds through the dimerization of the precursor, CO. To shed light on the factors contributing to the selective generation of C_{2+} in acidic solutions, studying CO electrolysis is more beneficial than studying CO_2 electrolysis. This is because the direct study on CO electrolysis allows for a constant amount of CO to be supplied to the catalytic surfaces and eliminates local pH variations caused by the dissolution of CO_2, thereby providing a more suitable environment to investigate important factors for CO dimerization in acidic electrolytes. However, the CO reduction reaction (CORR) to produce C_{2+} in acidic electrolytes has not been studied. In the present work, we quantitatively investigate the CORR to form C_{2+} products in an acidic solution through experimental gaseous CO electrolysis and numerical simulation of the local pH with the aim of identifying the necessary conditions for C_{2+} production.

2. Results and Discussion

2.1. Synthesis and Characterization of Cu Nanoparticles and GDEs Carrying Them

Copper nanoparticles (CuNPs) catalysts were synthesized using a chemical reduction method with $NaBH_4$ as the reductant (for details, refer to the Supporting Information). The crystal structures of the CuNPs were characterized by X-ray diffraction (XRD) analysis (Figure S1, Supporting Information). The XRD pattern shows peaks at 35.5° and 38.7°, which correspond to CuO(002) and CuO(111) planes. The Cu(II) oxidation state was also investigated by narrow-scan X-ray photoelectron spectroscopy (XPS) and X-ray absorption near edge structure (XANES) (Figures S2 and S3, Supporting Information). The narrow-scan Cu 2*p* XPS spectrum shows that both the Cu $2p_{3/2}$ and Cu $2p_{1/2}$ peaks at bonding energies of ≈933.8 and ≈953.7 eV contain signals from Cu(II). These results indicate that the surface of the CuNPs was almost oxidized by ambient air after synthesis. **Figure 1a** shows an SEM image of the CuNPs. Figure 1b,c show top-view and cross-sectional SEM images, respectively, of the CuNPs/GDE. Figure 1d shows an EDX mapping image corresponding to Figure 1c for Cu (the mapping images for other elements are shown in Figure S4, Supporting Information). The thickness of the CuNPs catalyst layer was 0.5–2 µm. The surface of the microporous layer (MPL) was almost fully covered by CuNPs.

2.2. CORR to Form C_{2+} Products in Acidic Electrolytes

For the CORR measurements, we used a custom-made three-compartment electrochemical cell (Figure S5, Supporting Information).[35,36] We obtain the current density versus potential curves of our electrode solution in pH 1.0 and 2.0 under continuous Ar or CO delivery conditions (Figure S6, Supporting Information). For all four conditions, the onset potential of cathodic currents was ≈−0.8 V versus Ag/AgCl. When Ar conditions were changed to CO conditions, the current values slightly decreased, which is likely due to the fact that adsorbed CO suppresses HER. The gaseous CORR products and liquid products were analyzed by gas chromatography and ^{1}H-NMR spectroscopy, respectively, after constant-current electrolysis (Figures S7 and S8, Supporting Information, respectively). The CORR products were analyzed at pH 1.0–14 under constant-current-density conditions. The K^+ concentration was fixed at 2.0 M in the series of experiments to eliminate the effect of alkali cations. The FEs for the CORR products in pH 2.0 solutions at different current densities are shown in **Figure 2a**. At the low current density of 50 mA cm^{-2}, the HER—the reaction that competes with the CORR—was dominant (FE_{H2} of 75%), whereas the FEs for CH_4 and C_{2+} from the CORR were 15% and less than 5%, respectively. The FE_{C2+} increased with increasing current density in the electrolyte at pH 2.0, reaching 75% at 200 mA cm^{-2}, and the main products were C_2H_4 (38%), ethanol (14%), acetic acid (17%), and *n*-propanol (6%) at 200 mA cm^{-2}. The FE_{C2+} did not substantially change even at 400 mA cm^{-2}. The partial current density for each product is shown in Figure 2b. The partial current density for C_{2+} production (j_{C2+}) increased monotonically to j_{C2+} = 280 mA cm^{-2} at J = 400 mA cm^{-2}. Approximately the same tendency was observed when the pH 1.0 solution was used as the electrolyte (Figure 2c,d). This is the first demonstration of CO reduction reaction to C_{2+} products at industrial current densities in acidic electrolytes. However, when the pH was lowered to 0.5, H_2 production became dominant even when the total current density was increased to 200 mA cm^{-2} (**Figure 3a**). The pH dependence of the CORR activity at 200 mA cm^{-2} (Figure 3a) revealed that although the increase was very slight above pH 7, the FE_{C2+} for CORR monotonically rises from pH 1.0 to pH 14. Although almost no FE_{C2+} was observed the HER was dominant at pH 0.5, and apparent C_{2+} formation (FE > 65%) occurred at pH 1.0–14.

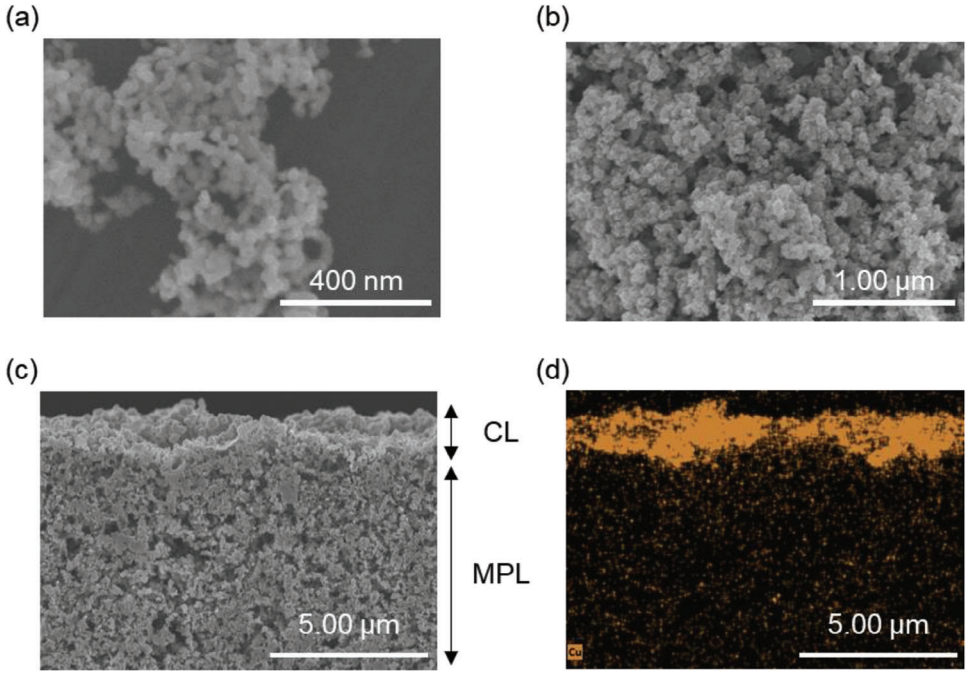

Figure 1. SEM image of a) CuNPs and b) CuNPs/GDE. c) Cross-sectional SEM image of CuNPs/GDE. d) The corresponding EDX mapping for Cu in the image (c).

2.3. Surface pH Simulation in Acidic Electrolytes

Given that the apparent C_{2+} formation was observed over a wide pH range (pH 1.0–14), we assume that the pH value at the surface of the catalyst layer (CL) increased substantially and became highly alkaline even when acidic or neutral electrolytes were used under high-rate electrolysis conditions. The alkalinity is attributed to both the CORR and HER being proton-consuming reactions. In addition, our group has shown that using a GDE enhances local proton depletion compared with the case where planar electrodes are used.[25] This assumption is also supported by the observation that the FE for C_{2+} increased with increasing current density.

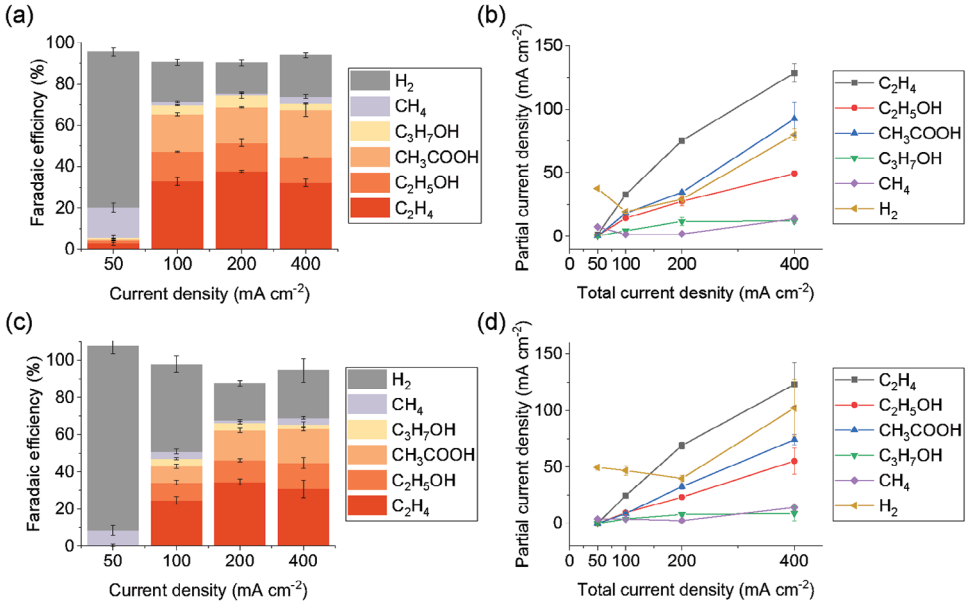

Figure 2. a) Faradaic efficiency and b) partial current density in pH 2.0 solution (0.5 M H_3PO_4 + 0.5 M KH_2PO_4 + 1.5 M KCl) at different current densities. c) Faradaic efficiency and d) partial current density in pH 1.0 solution (1.0 M H_3PO_4 + 2.0 M KCl) at different current densities.

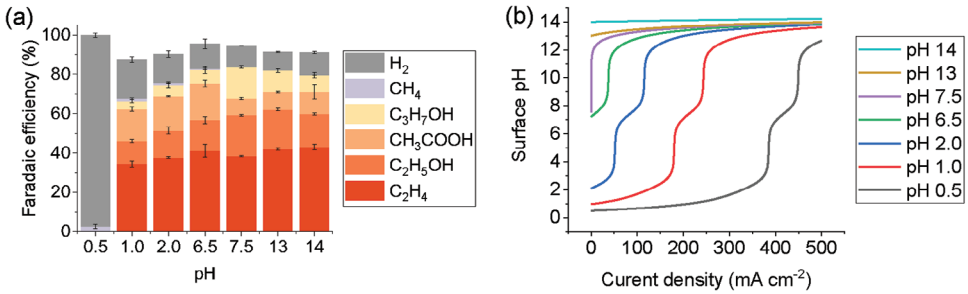

Figure 3. a) Faradaic efficiency at 200 mA cm^{-2} in electrolytes at various pH levels. The composition of each electrolyte is listed in Table S3 (Supporting Information). b) Simulation results of the surface pH (distance to the cathode of 0 μm). The current density was varied from 0 to 500 mA cm^{-2}. The electrolyte was the same as in the experiment in (a).

Thus, we next clarified the effect of local pH on the CORR under high-rate electrolysis using macro-scale theoretical simulations. The surface pH was simulated using the Reaction-Diffusion model.[37] A set of partial differential equations was solved using the finite element method implemented in the COMSOL Multiphysics environment. The thickness of the diffusion layer was set to 100 μm on the basis of previous reports.[18,31,38] For simplicity, we used a one-dimensional model with a point electrode and only considered the proton-consuming reaction, which can be rationalized because we can omit the pH alteration caused by CO_2 dissolution. Further details are provided in the Supporting Information. Figure 3b shows the theoretical surface pH as a function of the current density for various bulk pH levels. As predicted, the surface pH increased sharply at the current density threshold as a function of the bulk pH. The surface pH for a solution with a bulk pH of 2.0 increased to 3.8 at 50 mA cm^{-2} (i.e., the conditions were still acidic). For reactions in bulk pH 2.0 solutions, the surface pH crossed 7 at 70 mA cm^{-2} and the solution became strongly alkaline (12.9) at 200 mA cm^{-2}. This simulation result is basically in agreement with the experimental CORR results corresponding to pH 2.0 (Figure 2a). Specifically, the FE for C_{2+} dramatically increased from 5% at 50 to 70% at 100 mA cm^{-2}, reaching a value of 75% at 200 mA cm^{-2}. At pH 0.5, the surface remained acidic at 200 mA cm^{-2} (with a simulated surface pH of 0.95), which is consistent with the almost negligible production of C_{2+}. With respect to the results at pH 1.0, the simulation results indicate that the first and second pH jumps occur at 180 and 245 mA cm^{-2}, respectively. Meanwhile, the FE of C_{2+} production is 47% and 66% at 100 and 200 mA cm^{-2} at pH 1.0, respectively. While these results are qualitatively accurate, there is a slight quantitative discrepancy. This difference could be attributed to the need for an additional consideration of the local pH within the microscopic three-phase interface. We continue to investigate this aspect in our research lab and plan to report our findings in subsequent publications.

The simulated surface pH at 200 mA cm^{-2} was 0.9, 7.1. 13.0, 13.3, and 14.1 at bulk pH levels of 0.5, 1.0, 2.0, 6.5, and 14, respectively. These results are quantitatively consistent with the result that the HER dominates the CORR when the electrode surface is acidic. Thus, the change in surface pH is the most important factor for suppressing HER and for C—C bond formation.

2.4. Factors Affecting Surface Alkalization

As shown in the previous section, an increase in surface pH is critical for C_{2+} production by the CORR in acidic solutions. We next attempted to identify important factors for increasing the surface pH, focusing on the concentrations of alkali cations and on buffering effects. We first investigated the necessity of alkali cations for the CORR. **Figure 4a** shows the results for the CORR conducted in a pH 0.80 alkali cation-free electrolyte. In the absence of alkali cations, the predominant process observed was H_2 evolution. The only CORR product generated under these conditions was methane, albeit in minuscule amounts (FE_{CH4} = 0.2%); no C_{2+} products were detected. Figure 4b illustrates the simulation results reflecting the pH changes on the electrode surface while employing an electrolyte devoid of alkali cations. Irrespective of the increase in current density, the electrode surface maintains an acidic environment, suggesting that the system is unable to attain alkalinity because of a lack of counterbalancing positive charge against OH^-. Therefore, in the CORR processes involving acidic electrolytes, alkali cation species appear to facilitate local alkalization by serving as counter ions to the anions present on the electrode surface.

We then investigated the concentration dependence of the alkali cation species in the CORR. Figure 4c shows the FEs for CORR products at 200 mA cm^{-2} in pH 2.0 solutions in which the K^+ concentration was varied from 0.5 to 3.0 M by the addition of KCl. The FE_{C2+} exceeded 65% at all of the investigated K^+ concentrations and increased slightly with increasing K^+ concentration: from 69% at 0.5 to 83% at 3.0 M K^+. We used COMSOL to simulate the surface pH values in the presence of K^+ ions at various concentrations (Figure 4d). Although we observed that the pH jump from neutral to alkaline shifted to a lower current density with decreasing K^+ concentration, the concentration of K^+ had little effect on the surface pH compared with the bulk pH and the current density. In particular, the surface pH reached 13 at 200 mA cm^{-2} (experimental conditions), which coincides with the FE_{C2+} being consistently greater than 70% when the K^+ concentration is in the range of 0.5–3.0 M (Figure 4c). Namely, the alkali cation concentration is not the primary factor contributing to the surface alkalization, despite the slight increase in FE_{C2+} observed with an increase in K^+ concentration. The implications of the slight increase in FE_{C2+} with the increasing K^+ concentration will be discussed in the following section.

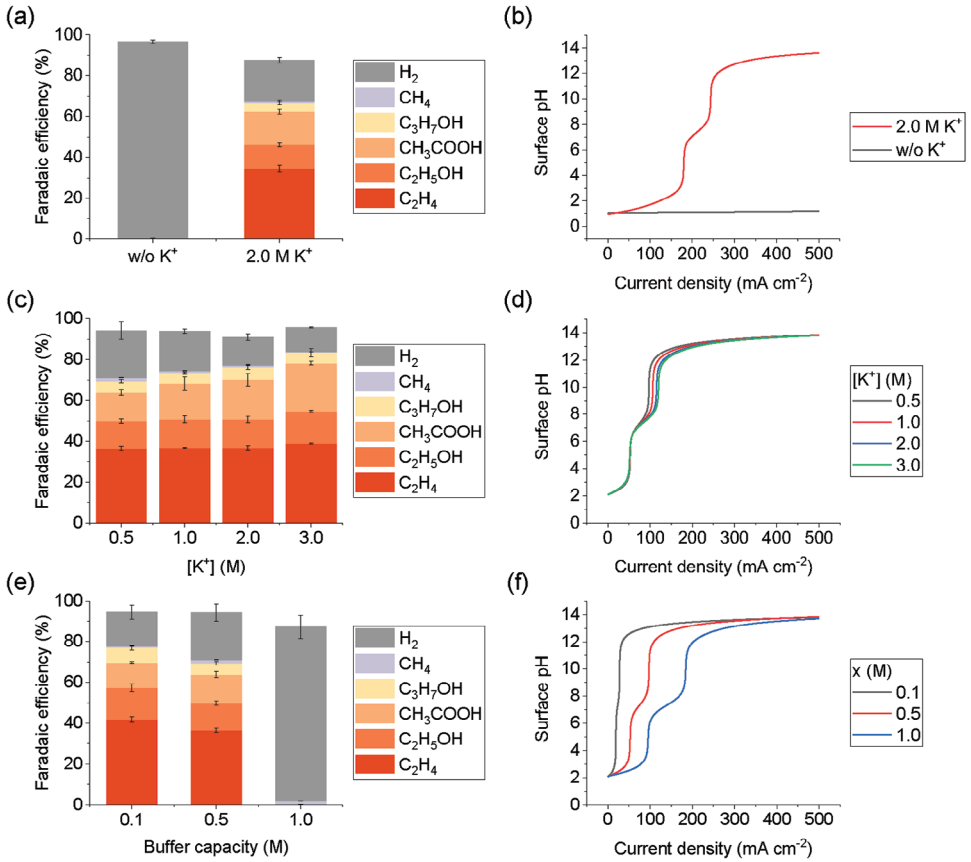

Figure 4. a) Faradaic efficiency in an alkali cation-free electrolyte (1.0 M H_3PO_4) at 200 mA cm^{-2}. b) Simulation results of the surface pH in an alkali cation-free electrolyte (1.0 M H_3PO_4). The results for a solution containing 2.0 M K^+ ions are shown for comparison. c) Faradaic efficiency in pH 2.0 solution with different K^+ concentrations (0.5 M H_3PO_4 + 0.5 M KH_2PO_4 + x M KCl, x = 0, 0.5, 1.5, 2.5) at 200 mA cm^{-2}. d) Simulation results for the surface pH. The electrolyte was the same as in the experiment in (c). e) Faradaic efficiency in pH 2.0 solution with different buffer capacities (x M H_3PO_4 + x M KH_2PO_4, x = 0.1, 0,5, 1.0) at 200 mA cm^{-2}. f) Simulation results for surface pH. The electrolyte was the same as in the experiment in (e).

Because the concentration of the buffer strongly affects local pH changes within the diffusion layer,[39,40] we next investigated the effect of a buffer on CORR activity by changing the phosphate species concentration. We prepared pH 2.0 solutions with 0.1, 0.5, and 1.0 M phosphates as electrolytes. Notably, although we also needed to change the K^+ concentration to maintain the bulk pH as the phosphate buffer concentration was varied, the K^+ concentration did not affect the CORR activity in this concentration range (Figure 4c). Figure 4e shows that the FE_{C2+} for the CORR at 200 mA cm^{-2} was 77% and 69% in 0.1 and 0.5 M phosphate solutions, respectively. However, when the phosphate concentration was increased to 1.0 M, the HER became dominant and C_{2+} formation was scarcely observed. As the buffering capacity increased with increasing concentration of phosphate anions, the pH jump threshold shifted toward higher current density. Although the surface apparently became alkaline at 200 mA cm^{-2} in 0.1 and 0.5 M phosphate solutions (bulk pH 2.0), the current density of 200 mA cm^{-2} was just at the threshold for the pH jump in 1.0 M phosphate solutions (Figure 4f). These simulation results suggest that alkalization of the surface would not be sufficient for an effective CORR in 1.0 M phosphate solutions in the experiment, consistent with the experimental CORR results (Figure 4e).

2.5. Factors Affecting C_{2+} Selectivity After Surface Alkalization

In the previous sections, alkalization of the electrode surface was shown to be required to suppress the HER and selectively generate C_{2+} products. Therefore, we next investigated the factors that further influence the selectivity for C_{2+} products when alkalinized. As shown in Figure 4c, we observed a slight increase in FE_{C2+} with a rising amount of K^+, even though the surface pH remained constant. We assumed that this slight increase in FE_{C2+} is due to the stabilization effect of surface alkali cations on the adsorbed CO molecules. Previous theoretical and experimental studies have shown that adsorbed CO molecules are coordinated and stabilized by alkali cations, promoting CO dimerization.[32,41–43] (please see the next section) To investigate this hypothesis, we replaced K^+ with Na^+ ions in the electrolyte. Although the surface pH did not depend on the alkali cation species (**Figure 5b**), the FE_{C2+} in Na^+ solutions was much lower than that in K^+ solutions (Figure 5a). We observed the apparent difference of FE among K^+ and Na^+ even when using 1.0 M H_3PO_4 + 1.3 M *M*Cl + 0.7 M *M*OH (for the detail, see Figure S9, Supporting Information and its caption). In addition to the alkali cation species dependence of the CORR, given that the surface K^+ concentration depends on the bulk K^+

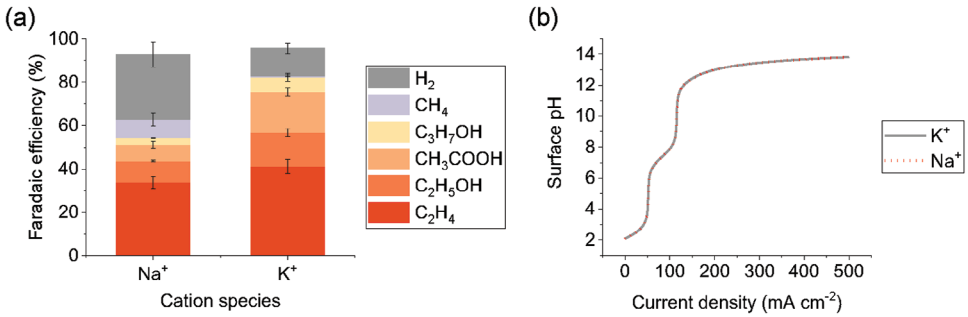

Figure 5. a) Faradaic efficiency in pH 2.0 solution containing different cation species (0.5 M H_3PO_4 + 0.5 M H_2PO_4 + 1.5 M *M*Cl, *M* = Na^+, K^+) at 200 mA cm^{-2}. b) Simulation results for surface pH. The electrolyte was the same as in the experiment in (a).

concentration (Figure S10, Supporting Information), the surface K^+ would facilitate CO dimerization, resulting in a slight increase in FE_{C2+} with increasing bulk K^+ concentration.

2.6. Discussion About C_{2+} Formation in Acidic Electrolyte

Our CORR experiments and simulation results indicate that local alkalinity at pH levels greater than seven is an absolute requirement for selective C_{2+} formation (FE_{C2+} > 60%). In addition, when local alkalinity is achieved, the concentration and species of alkali cations influence the selectivity for C_{2+} production (**Figure 6**, left). Here, let us consider the mechanism of these trends. First, we can explain the requirement of alkaline conditions for C_{2+} formation as follows. There are mainly two possible mechanisms by which C_{2+} formation is enhanced by the local alkaline environment. First, whereas the rate and theoretical potential for H_2 formation are clearly dependent on proton activity, the rate-determining step (RDS) for the reduction of CO or CO_2 to C_{2+} is suggested to be unrelated to proton addition. Despite also being a proton-consuming reaction, Wang and colleagues demonstrated that C_{2+} formation during CO_2RR catalyzed by polycrystalline copper occurs independently of pH when measured on a standard hydrogen electrode (SHE) scale.[44] Additionally, Kastlunger et al. showed that the dimerization of CO is an RDS based on the experimental results of CORR and constant-potential density functional theory.[45] Based on these studies, H_2 evolution would be selectively suppressed and C_{2+} formation would become relatively dominant under alkaline conditions. Another possible explanation is that hydroxide ions facilitate the formation of C_{2+}. For instance, the presence of OH^- ions can reduce the activation energy required for C—C coupling, as indicated by DFT studies.[46,47] This effect is attributed to the increased charge imbalance between carbon atoms in the adsorbed OCCO species, leading to a more stable intermediate due to enhanced dipole attraction.[46] Furthermore, Sun et al. provided experimental evidence that electrodes with higher amounts of OH exhibit enhanced selectivity for C_{2+} by fabricating OH/Cu electrodes with varying amounts of OH adsorption.[48] As a future work, we would like to elucidate the detailed mechanism using both experimental and computational studies.

Next, we discuss the effect of the concentration and species of alkali cation on C_{2+} selectivity after surface alkalization (Figure 6, right). It has been reported that alkali cations have the effect of stabilizing the intermediate species for C_{2+}. For example, alkali cations have been shown to directly coordinate with the OCCO intermediate, as evidenced by ab initio molecular dynamics (AIMD).[41] The free energy for the dimerization of CO was

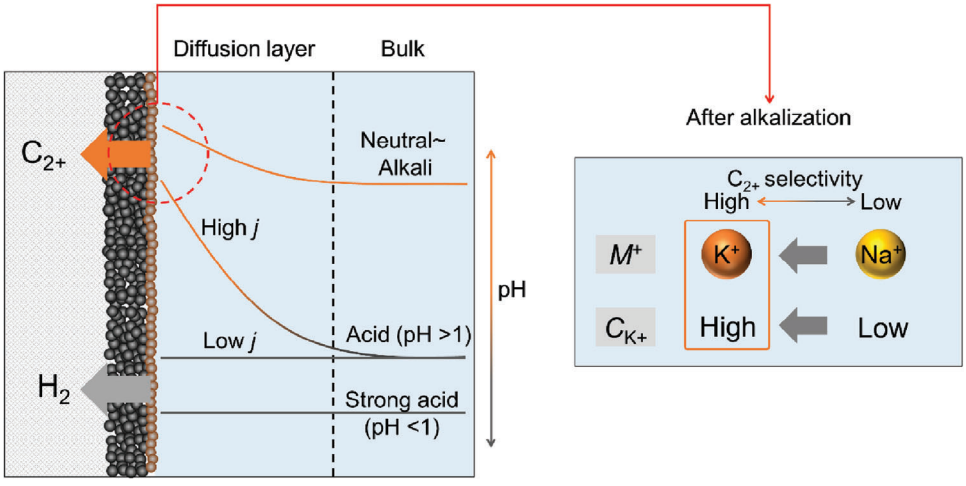

Figure 6. Schematic of electrode vicinity during electrochemical CO reduction. This figure shows the relationship between local pH and product selectivity.

reduced as the radius of the coordinating alkali cations increased. The other reported effect of alkali cations on the dimerization of CO is due to the modulation of the interfacial electric field. Resasco et al. observed an increase in the partial current density for C_{2+} (ethylene and ethanol) during CO_2RR on Cu electrodes with increasing the radius of alkali cations in electrolytes.[42] They attributed this effect to the stabilization of the intermediate by the interfacial electric field, which is dependent on the cation radius. Additionally, Ringe and colleagues, using an ab initio/continuum approach, reported that weakly hydrated cations such as K^+ and Cs^+ tend to accumulate at the outer Helmholtz plane.[43] Consequently, the presence of these cations in the electrolyte results in an increased surface positive charge density, leading to a stronger interfacial electric field. In this study as well, the effects exerted by these alkali cation species on the reaction intermediates likely modulated the C_{2+} production selectivity after surface alkalization.

3. Conclusion

In conclusion, we attained C_{2+} production through the CORR in highly acidic solutions with a pH of 1.0 or 2.0. The achievement of local alkalinity with a pH > 7 at the electrode surfaces, which is a result of electrochemical proton-consuming reactions (i.e., the CORR and HER), is a requirement for C_{2+} production (FE_{C2+} > 60%). Through numerical calculations and CORR experiments, we found that the local pH is primarily influenced by the bulk pH and the current density. Once alkalinity was achieved, the concentration and species of alkali cations became the determining factors affecting the selectivity for C_{2+} production. Achieving efficient C_{2+} formation via the CO_2RR in an acidic electrolyte is beneficial from the viewpoints of carbon and energy efficiency because neutral and alkaline solutions absorb CO_2 as (bi)carbonate, and substantial energy is required to convert (bi)carbonates back into CO_2. In addition, the practical implementation of CO_2RR requires a membrane electrode assembly (MEA)-type cell, similar to the implementation for water electrolysis. Currently, only systems equipped with anion-exchange membranes can generate C_{2+} in MEA-type CO_2 electrolysis. Therefore, the use of a more robust and highly conductive acidic proton-exchange membrane to establish MEA-type CO_2 electrolysis is desirable. The novel insights obtained in this study are expected to contribute to the development of an MEA-type CO_2 electrolysis system equipped with proton-exchange membranes.

Supporting Information

Supporting Information is available from the Wiley Online Library or from the author.

Acknowledgements

This research was based on the Integrated Electrochemical Systems for Scalable CO_2 Conversion to Chemical Feedstocks project performed as part of the Moonshot Research and Development Program funded by the New Energy and Industrial Technology Development Organization (Grant no. 20001627-0). This work was also supported by a JSPS KAKENHI Program (Grant no. 23H02063) and CREST (Grant no. JPMJCR18R3) of the Japan Science and Technology Agency (JST). Synchrotron radiation experiments were performed using the BL01B1 beamline of SPring-8 with the approval of the Japan Synchrotron Radiation Research Institute (Proposals 2022B0566, 2023A1690, and 2023A1934).

Conflict of Interest

The authors declare no conflict of interest.

Data Availability Statement

The data that support the findings of this study are available from the corresponding author upon reasonable request.

Keywords

acidic electrolyte, CO reduction reactions, gas-diffusion electrodes, high-rate electrolysis, numerical simulation

Received: September 1, 2023
Revised: November 16, 2023
Published online:

[1] K. Kamiya, K. Fujii, M. Sugiyama, S. Nakanishi, *Chem. Lett.* **2021**, *50*, 166.
[2] W. Zhang, Y. Hu, L. Ma, G. Zhu, Y. Wang, X. Xue, R. Chen, S. Yang, Z. Jin, *Adv. Sci.* **2018**, *5*, 1700275.
[3] S. Nitopi, E. Bertheussen, S. B. Scott, X. Liu, A. K. Engstfeld, S. Horch, B. Seger, I. E. L. Stephens, K. Chan, C. Hahn, J. K. Nørskov, T. F. Jaramillo, I. Chorkendorff, *Chem. Rev.* **2019**, *119*, 7610.
[4] Z. W. Seh, J. Kibsgaard, C. F. Dickens, I. Chorkendorff, J. K. Nørskov, T. F. Jaramillo, *Science* **2017**, *355*, eaad4998.
[5] P. De Luna, C. Hahn, D. Higgins, S. A. Jaffer, T. F. Jaramillo, E. H. Sargent, *Science* **2019**, *364*, eaav3506.
[6] J. M. Spurgeon, B. Kumar, *Energy Environ. Sci.* **2018**, *11*, 1536.
[7] M. G. Kibria, J. P. Edwards, C. M. Gabardo, C.-T. Dinh, A. Seifitokaldani, D. Sinton, E. H. Sargent, *Adv. Mater.* **2019**, *31*, 1807166.
[8] Y. Zhou, A. J. Martín, F. Dattila, S. Xi, N. López, J. Pérez-Ramírez, B. S. Yeo, *Nat. Catal.* **2022**, *5*, 545.
[9] F. Pan, X. Yang, T. O'carroll, H. Li, K.-J. Chen, G. Wu, *Adv. Energy Mater.* **2022**, *12*, 2200586.
[10] Y. Hori, K. Kikuchi, S. Suzuki, *Chem. Lett.* **1985**, *14*, 1695.
[11] Y. Hori, K. Kikuchi, A. Murata, S. Suzuki, *Chem. Lett.* **1986**, *15*, 897.
[12] A. Bagger, W. Ju, A. S. Varela, P. Strasser, J. Rossmeisl, *ChemPhysChem* **2017**, *18*, 3266.
[13] *Electrochim. Acta* **1994**, *39*, 1833.
[14] Y. Zheng, A. Vasileff, X. Zhou, Y. Jiao, M. Jaroniec, S.-Z. Qiao, *J. Am. Chem. Soc.* **2019**, *141*, 7646.
[15] F. P. García De Arquer, C.-T. Dinh, A. Ozden, J. Wicks, C. Mccallum, A. R. Kirmani, D.-H. Nam, C. Gabardo, A. Seifitokaldani, X. Wang, Y. C. Li, F. Li, J. Edwards, L. J. Richter, S. J. Thorpe, D. Sinton, E. H. Sargent, *Science* **2020**, *367*, 661.
[16] T. Möller, T. Ngo Thanh, X. Wang, W. Ju, Z. Jovanov, P. Strasser, *Energy Environ. Sci.* **2021**, *14*, 5995.
[17] M. Ma, E. L. Clark, K. T. Therkildsen, S. Dalsgaard, I. Chorkendorff, B. Seger, *Energy Environ. Sci.* **2020**, *13*, 977.
[18] J. Gu, S. Liu, W. Ni, W. Ren, S. Haussener, X. Hu, *Nat. Catal.* **2022**, *5*, 268.
[19] J. A. Rabinowitz, M. W. Kanan, *Nat. Commun.* **2020**, *11*, 5231.

[20] A. Inoue, T. Harada, S. Nakanishi, K. Kamiya, *EES. Cata.* **2023**, *1*, 9.
[21] T. Burdyny, W. A. Smith, *Energy Environ. Sci.* **2019**, *12*, 1442.
[22] Z. Xing, L. Hu, D. S. Ripatti, X. Hu, X. Feng, *Nat. Commun.* **2021**, *12*, 136.
[23] J. E. Huang, F. Li, A. Ozden, A. Sedighian Rasouli, F. P. García De Arquer, S. Liu, S. Zhang, M. Luo, X. Wang, Y. Lum, Y. Xu, K. Bertens, R. K. Miao, C.-T. Dinh, D. Sinton, E. H. Sargent, *Science* **2021**, *372*, 1074.
[24] Z. Ma, Z. Yang, W. Lai, Q. Wang, Y. Qiao, H. Tao, C. Lian, M. Liu, C. Ma, A. Pan, H. Huang, *Nat. Commun.* **2022**, *13*, 7596.
[25] Y. Wu, K. Kamiya, T. Hashimoto, R. Sugimoto, T. Harada, K. Fujii, S. Nakanishi, *Electrochemistry* **2020**, *88*, 359.
[26] H. Ooka, M. C. Figueiredo, M. T. M. Koper, *Langmuir* **2017**, *33*, 9307.
[27] Z. Wang, P. Hou, Y. Wang, X. Xiang, P. Kang, *ACS Sustainable Chem. Eng.* **2019**, *7*, 6106.
[28] C. J. Bondue, M. Graf, A. Goyal, M. T. M. Koper, *J. Am. Chem. Soc.* **2021**, *143*, 279.
[29] M. C. O. Monteiro, M. F. Philips, K. J. P. Schouten, M. T. M. Koper, *Nat. Commun.* **2021**, *12*, 4943.
[30] Y. Qiao, W. Lai, K. Huang, T. Yu, Q. Wang, L. Gao, Z. Yang, Z. Ma, T. Sun, M. Liu, C. Lian, H. Huang, *ACS Catal.* **2022**, *12*, 2357.
[31] Y. Xie, P. Ou, X. Wang, Z. Xu, Y. C. Li, Z. Wang, J. E. Huang, J. Wicks, C. Mccallum, N. Wang, Y. Wang, T. Chen, B. T. W. Lo, D. Sinton, J. C. Yu, Y. Wang, E. H. Sargent, *Nat. Catal.* **2022**, *5*, 564.
[32] Z. Xu, M. Sun, Z. Zhang, Y. Xie, H. Hou, X. Ji, T. Liu, B. Huang, Y. Wang, *ChemCatChem* **2022**, *14*, 202200052.
[33] X. Sheng, W. Ge, H. Jiang, C. Li, *Adv. Mater.* **2022**, *34*, 2201295.
[34] W. Nie, G. P. Heim, N. B. Watkins, T. Agapie, J. C. Peters, *Angew. Chem. Int. Ed Engl.* **2023**, *62*, 202216102.
[35] Y. Wu, K. Iwase, T. Harada, S. Nakanishi, K. Kamiya, *ACS Appl. Nano Mater* **2021**, *4*, 4994.
[36] R. Kato, J. H. Lettow, S. N. Patel, S. J. Rowan, *ACS Appl. Mater. Interfaces* **2020**, *12*, 54083.
[37] N. Gupta, M. Gattrell, B. Macdougall, *J. Appl. Electrochem.* **2006**, *36*, 161.
[38] Y. Chen, N. S. Lewis, C. Xiang, *J. Electrochem. Soc.* **2020**, *167*, 114503.
[39] K. Obata, R. Van De Krol, M. Schwarze, R. Schomäcker, F. F. Abdi, *Energy Environ. Sci.* **2020**, *13*, 5104.
[40] P. Bollella, A. Melman, E. Katz, *ChemElectroChem* **2021**, *8*, 3923.
[41] H. Liu, J. Liu, B. Yang, *ACS Catal.* **2021**, *11*, 12336.
[42] J. Resasco, L. D. Chen, E. Clark, C. Tsai, C. Hahn, T. F. Jaramillo, K. Chan, A. T. Bell, *J. Am. Chem. Soc.* **2017**, *139*, 11277.
[43] S. Ringe, E. L. Clark, J. Resasco, A. Walton, B. Seger, A. T. Bell, K. Chan, *Energy Environ. Sci.* **2019**, *12*, 3001.
[44] L. Wang, S. A. Nitopi, E. Bertheussen, M. Orazov, C. G. Morales-Guio, X. Liu, D. C. Higgins, K. Chan, J. K. Nørskov, C. Hahn, T. F. Jaramillo, *ACS Catal.* **2018**, *8*, 7445.
[45] G. Kastlunger, L. Wang, N. Govindarajan, H. H. Heenen, S. Ringe, T. Jaramillo, C. Hahn, K. Chan, *ACS Catal.* **2022**, *12*, 4344.
[46] C.-T. Dinh, T. Burdyny, M. G. Kibria, A. Seifitokaldani, C. M. Gabardo, F. P. García De Arquer, A. Kiani, J. P. Edwards, P. De Luna, O. S. Bushuyev, C. Zou, R. Quintero-Bermudez, Y. Pang, D. Sinton, E. H. Sargent, *Science* **2018**, *360*, 783.
[47] Y. Cao, Z. Chen, P. Li, A. Ozden, P. Ou, W. Ni, J. Abed, E. Shirzadi, J. Zhang, D. Sinton, J. Ge, E. H. Sargent, *Nat. Commun.* **2023**, *14*, 70.
[48] M. Sun, A. Staykov, M. Yamauchi, *ACS Catal.* **2022**, *12*, 14856.